

Identification of Young Stellar Variables with KELT for *K2* II: The Upper Scorpius Association

Megan Ansdell¹, Ryan J. Oelkers², Joseph E. Rodriguez³, Eric Gaidos⁴,
Garrett Somers², Eric Mamajek^{5,6}, Phillip A. Cargile³, Keivan G. Stassun^{2,7},
Joshua Pepper⁸, Daniel J. Stevens⁹, Thomas G. Beatty^{10,11}, Robert J. Siverd¹²,
Michael B. Lund², Rudolf B. Kuhn¹³, David James¹⁴, B. Scott Gaudi⁸

¹*Institute for Astronomy, University of Hawai'i at Mānoa, 2680 Woodlawn Dr, Honolulu, HI 96822, USA*

²*Department of Physics and Astronomy, Vanderbilt University, 6301 Stevenson Center, Nashville, TN 37235, USA*

³*Harvard-Smithsonian Center for Astrophysics, 60 Garden St, Cambridge, MA 02138, USA*

⁴*Department of Geology & Geophysics, University of Hawai'i at Mānoa, Honolulu, HI 96822, USA*

⁵*Jet Propulsion Laboratory, California Institute of Technology, M/S 321-100, 4800 Oak Grove Dr, Pasadena, CA 91109, USA*

⁶*Department of Physics and Astronomy, University of Rochester, Rochester, NY 14627, USA*

⁷*Department of Physics, Fisk University, 1000 17th Avenue North, Nashville, TN 37208, USA*

⁸*Department of Physics, Lehigh University, 16 Memorial Drive East, Bethlehem, PA 18015, USA*

⁹*Department of Astronomy, The Ohio State University, Columbus, OH 43210, USA*

¹⁰*Department of Astronomy & Astrophysics, The Pennsylvania State University, 525 Davey Lab, University Park, PA 16802, USA*

¹¹*Center for Exoplanets and Habitable Worlds, The Pennsylvania State University, 525 Davey Lab, University Park, PA 16802, USA*

¹²*Las Cumbres Observatory Global Telescope Network, 6740 Cortona Dr., Suite 102, Santa Barbara, CA 93117, USA*

¹³*South African Astronomical Observatory, PO Box 9, Observatory 7935, South Africa*

¹⁴*Astronomy Department, University of Washington, Box 351580, Seattle, WA 98195, USA*

Submitted to MNRAS on 23 July 2017

ABSTRACT

High-precision photometry from space-based missions such as *K2* and *TESS* enables detailed studies of young star variability. However, because space-based observing campaigns are often short (e.g., 80 days for *K2*), complementary long-baseline photometric surveys are critical for obtaining a complete understanding of young star variability, which can change on timescales of minutes to years. We therefore present and analyze light curves of members of the Upper Scorpius association made over 5.5 years by the ground-based Kilodegree Extremely Little Telescope (KELT), which complement the high-precision observations of this region taken by *K2* during its Campaigns 2 and 15. We show that KELT data accurately identify the periodic signals found with high-precision *K2* photometry, demonstrating the power of ground-based surveys in deriving stellar rotation periods of young stars. We also use KELT data to identify sources exhibiting variability that is likely related to circumstellar material and/or stellar activity cycles; these signatures are often unseen in the short-term *K2* data, illustrating the importance of long-term monitoring surveys for studying the full range of young star variability. We provide the KELT light curves as electronic tables in an ongoing effort to establish legacy time-series datasets for young stellar clusters.

Key words: stars: pre-main sequence – stars: variables – variables: T Tauri

1 INTRODUCTION

Young stars have long been known to exhibit diverse photometric variability attributed to a range of physical mechanisms (see an early review in Bertout 1989). Classical T Tauri stars (CTTS) are characterized by their full disks and ongoing accretion, which translate into an array of complicated light curve features (e.g., Cody et al. 2014). In par-

ticular, very deep dimming events lasting days to months have been connected to various forms of occulting disk structures (e.g., Bouvier et al. 1999; Dullemond et al. 2003; Cody et al. 2014; Ansdell et al. 2016b). Flaring events related to accretion bursts are also common, especially for magnetically active, rapidly rotating stars. More evolved weak-line T Tauri stars (WTTS), which no longer host significant disks

or show clear accretion signatures, typically exhibit sinusoidal variability in their light curves, attributable to spots on the stellar surface rotating with the star. These sinusoidal variations can be used to estimate stellar rotation periods, which lengthen over the first few hundred Myr of evolution as stars spin down via magnetized stellar winds that remove angular momentum (Herbst et al. 2007). Recently, WTTS have also been found to display long-term variability in their brightness, possibly due to magnetic activity cycles (Rodríguez et al. 2017b).

Thus studying the photometric variability of young stars can give insight into stellar evolution as well as the structure and dynamics of the surrounding circumstellar material as it presumably forms planets. Much of what we know about the variability of young stars comes from all-sky ($\gtrsim 70\%$), long-baseline (\sim years), high-cadence (10s of minutes) photometric monitoring surveys from the ground (e.g., ASAS, CRTS, WASP, KELT, ASAS-SN; Pojmanski 1997; Drake et al. 2009; Pollacco et al. 2006; Pepper et al. 2007, 2012) as well as generally shorter-term but much higher-precision monitoring by space-based missions (e.g., CoRoT, *Spitzer*/IRAC, *Kepler*, *K2*; Fazio et al. 2004; Baglin et al. 2006; Borucki et al. 2010; Howell et al. 2014).

The Upper Scorpius association (Upper Sco) is a particularly interesting target for studies of young star variability, as it is the nearest star-forming region (145 pc; de Zeeuw et al. 1999) with a median age (≈ 5 –11 Myr; Preibisch et al. 2002; Pecaú et al. 2012) that is comparable to the disk dispersal timescale (Williams & Cieza 2011). Moreover, its population of several hundred stars and brown dwarfs has been well studied at various wavelengths. In particular, its disk population has been characterized in the infrared by *Spitzer* (Carpenter et al. 2006) and WISE (Luhman & Mamajek 2012) as well as in the sub-mm by ALMA (Carpenter et al. 2014; Barenfeld et al. 2016). Stars in this association have also been surveyed for multiplicity using ground-based adaptive optics (e.g., Kraus et al. 2008; Lafrenière et al. 2014). Additionally, the re-purposed space-based *Kepler* mission, *K2* (Howell et al. 2014), has provided high-precision time-series photometry during its Campaign 2 (C2), leading to numerous studies of young star variability in Upper Sco (e.g., Ripepi et al. 2015; Ansdell et al. 2016b; Scaringi et al. 2016; Cody et al. 2017; Stauffer et al. 2017). *K2* will visit another field that partially overlaps with Upper Sco in its upcoming Campaign 15 (C15) planned for 23 August to 20 November 2017, providing yet another opportunity to study young star variability in this association.

The space-based *K2* observing campaigns last 80 days and the data are not available until months after they are taken. Thus, from *K2* data alone, it is challenging to discern variability on timescales much longer than a month. Moreover, because the photometric variability of the targeted stars is often not known in advance, it is difficult to complement *K2* observations with simultaneous spectroscopy or multi-passband photometry, which can be critical to identifying the mechanisms driving young star variability (e.g., Zhang et al. 2015). Fortunately, long-term ground-based photometric surveys can identify variables in advance of space-based monitoring campaigns as well as extend the observing baselines to nearly a decade or more in many cases.

To this end, we are providing ground-based photometry of young stellar clusters taken by the Kilodegree Ex-

tremely Little Telescope (KELT) in an effort to establish legacy time-series datasets for studying young star variability. KELT provides long-baseline ($\lesssim 10$ yr) high-cadence (10–20 min) photometry at $\sim 1\%$ precision for bright ($7 < V < 11$) stars across the sky, making it well-suited to studying photometric variability of young star-disk systems on timescales of days to years. In Part I of this series, we provided KELT light curves of Taurus-Auriga members targeted by *K2* (Rodríguez et al. 2017a); here in Part II, we extend this work to Upper Sco members also targeted by *K2*. In Section 2.1 we present our sample and in Section 2.2 we describe the KELT observations. The variability and periodicity of the sample are assessed in Section 2.3, then discussed in terms of young star-disk variability in Sections 3 and 4. We summarize our work in Section 5.

2 DATA & METHODS

2.1 Target Selection

Our sample of candidate Upper Sco members is compiled by merging the catalogues of Luhman & Mamajek (2012), Rizzuto et al. (2015), and Pecaú & Mamajek (2016). We also include the stars identified by Preibisch et al. (1998) as candidate young cluster members, but caution that their Upper Sco membership is highly uncertain due to their weak lithium absorption. These catalogues were selected using proper motions cuts and/or diagnostics of youth (e.g., infrared excess, lithium absorption, X-ray emission). We do not make any additional selection cuts in order to provide as broad a sample as possible.

We find that 148 candidate Upper Sco members have matches in the KELT survey and also fall on working *K2* detectors in C2 or C15. Due to the brightness limit of the KELT survey (see Section 2.2), these stars are biased toward Upper Sco members with $M_{\star} \gtrsim 0.5 M_{\odot}$. All of these sources have near-infrared counterparts in the Two Micron All-Sky Survey (2MASS; Skrutskie et al. 2006), thus we use 2MASS names for identification throughout this work. To respect the saturation limit in the KELT-South data, we also make an optical magnitude cut of $V > 8$ mag, resulting in a final sample of 131 targets presented in Table 1.

2.2 KELT Observations

The KELT survey is designed to discover giant planets transiting bright ($7 < V < 11$ mag) host stars. KELT consists of two telescopes, each with a 42-mm telephoto lens, with KELT-North at the Winer Observatory in Arizona (United States) and KELT-South at the South African Astronomical Observatory in Sutherland (South Africa). Each KELT telescope uses a Paramount ME German equatorial mount that requires 180-degree rotations when passing the meridian. Because the telescope optics are not axisymmetric, the stellar point-spread function (PSF) changes from east to west observing orientations; east and west observations are therefore treated as two separate telescopes during the data reduction process. Together, the two telescopes observe over 70% of the sky with 10- to 30-min cadence. Each telescope uses a broad *R*-band filter ($\lambda_{\text{eff}} = 691$ nm, $W_{\text{eff}} = 318$ nm; Pepper et al. 2007) and has a $26^{\circ} \times 26^{\circ}$ field of view with

a 23'' pixel scale. The typical photometric error for bright ($7 < V < 11$ mag) stars is 1%, however the telescopes also obtain lower-precision photometry of stars as faint as $V \approx 14$ mag (Pepper et al. 2007, 2012). See Siverd et al. (2012) and Kuhn et al. (2016) for detailed descriptions of the KELT observing strategy and data reduction process.

The KELT data used in this work are from the KELT-South field 26 (KS-26), which is centered at $\alpha = 15^h 19^m 48^s$, $\delta = -20^\circ 00' 00''$ (J2000). The KELT light curves for all 131 stars in our sample are available as electronic tables via Filtergraph (Burger et al. 2013).¹ The single-point photometric error on the data depends on the target brightness, but is typically < 0.05 mag. The first KELT-South season has a known systematic associated with telescope focusing, thus any long-term changes in brightness that are seen only in this first season should be viewed with extreme caution. Due to the large pixel scale of KELT, some of the targets in our sample may also be blended into a single KELT light curve; we flag 27 sources as possible blends in Table 1 due to another star with similar brightness (± 1.5 mag) being located within $2'$ (≈ 5 KELT pixels).

2.3 Variability & Periodicity Tests

2.3.1 Variability Testing

We identify variable sources in our sample by applying four metrics to all the light curves from KS-26, following the work of Wang et al. (2013) and Oelkers et al. (2015). As shown in Figure 1, these metrics identify sources with variability amplitudes that are large relative to other stars within the same field, where the variability is not necessarily periodic. We outline each variability metric below, but direct the reader to the previously cited works for more detailed discussions.

We identify candidate variables with light curves exhibiting unusually high dispersion for their magnitude using the rms and Δ_{90} statistics. The rms statistic identifies the magnitude range for 68% of the data points in a light curve, whereas the Δ_{90} statistic identifies the magnitude range for 90% of the data points in a light curve. Using all the light curves from KS-26, we compute the upper 2σ envelopes of both statistics as a function of magnitude, then flag objects in our sample lying above these limits as candidate variables (see top panels in Figure 1). In order to define the envelopes using stars with minimal variability, we apply a 2.5σ iterative clipping to the sample prior to defining the envelope.

We also compute the Welch-Stetson J and L statistics (Stetson 1996), which were designed to identify objects that show correlations in their residuals from the mean with time. As shown in Figure 1 (middle panels), these statistics are expected to produce a distribution of values centered at or near zero with a one-sided tail containing the variable objects. These statistics perform well on data from the KELT survey due to its high cadence over long time baselines. We compute the $+3\sigma$ cutoff of the tail in J , and the $+5\sigma$ cutoff of the tail in L , to identify candidate variables. We apply a more stringent cutoff in L because this helps to remove the spurious variables that pass the other three metrics but show

features of known detector systematics, while still retaining objects that show variations consistent with astrophysical phenomena. In order to calculate the cutoffs for J and L based on stars showing minimal light curve variations, we remove objects with $J, L > 3$ and perform a 2.5σ iterative clipping prior to calculating the mean and standard deviation values of the J and L distributions.

Figure 1 shows the distributions of the four metrics for all sources in KS-26 as well as the cutoffs for identifying candidate variables in our sample. Sources passing all four metrics are flagged as variables in Table 1, which also gives the rms statistic for each source as an estimate of the variability amplitude. We note that the proximity of KS-26 to the galactic bulge means that these amplitudes may be diluted due to blending.

2.3.2 Periodicity Testing

We search each KELT light curve for periodic signals between 0.1 and 150 days using the Lomb-Scargle periodogram (LSP; Lomb 1976; Scargle 1982) as implemented in the `AstroPy` Python library.² We reject periods if the power in the periodogram is < 0.02 , or if the period is within 5% of a solar day or 2% of its first 10 harmonics ($f, f/2, f/3, \dots$) to avoid aliases associated with the diurnal cycle. We also reject periods between 26 and 30 days to avoid aliases associated with the lunar cycle, which arise because Moon glow can produce time-correlated noise by regularly increasing the sky background, even for sources separated from the Moon by dozens of degrees. Additionally, we reject periods for which $2\times$ or $0.5\times$ the period fails any of the alias checks described above.

The period with the highest power fulfilling the above criteria is listed in Table 1 for each target. If no period is listed, then no significant period could be found for that target. The phase-folded light curves for the sources with identified periods are shown in Figure 2. We do not report any lower-power periods fulfilling the above criteria, as we find that the highest-power periods derived from KELT data consistently match the periods derived from the much higher-precision *K2/C2* data (see Section 4.1). As an additional check, we execute a boot-strap analysis using 1000 Monte-Carlo iterations, where for each iteration the observation dates are unchanged but the magnitude values are randomly shuffled (Henderson & Stassun 2012). We calculate the LSP for each iteration and record the peak power; if the maximum peak power is larger than the power of the period found using the original light curve, we reject the period as a false positive signal. We note that none of the periods derived above were rejected during this additional screening process.

We find periodic signals in the KELT data for 89 sources in our sample. The vast majority of these periodic signals are consistent with the rotation of spots on the surfaces of low-mass stars that are ≈ 10 Myr old. More specifically, they have periods of ≈ 0.5 –10 days with amplitudes of a few percent (e.g., Herbst et al. 2007). The handful of targets exhibiting more exotic variability are discussed in the following section.

¹ https://filtergraph.com/kelt_k2 (this link also includes KELT data for other papers in this series; Rodriguez et al. 2017a).

² <http://www.astropy.org/>

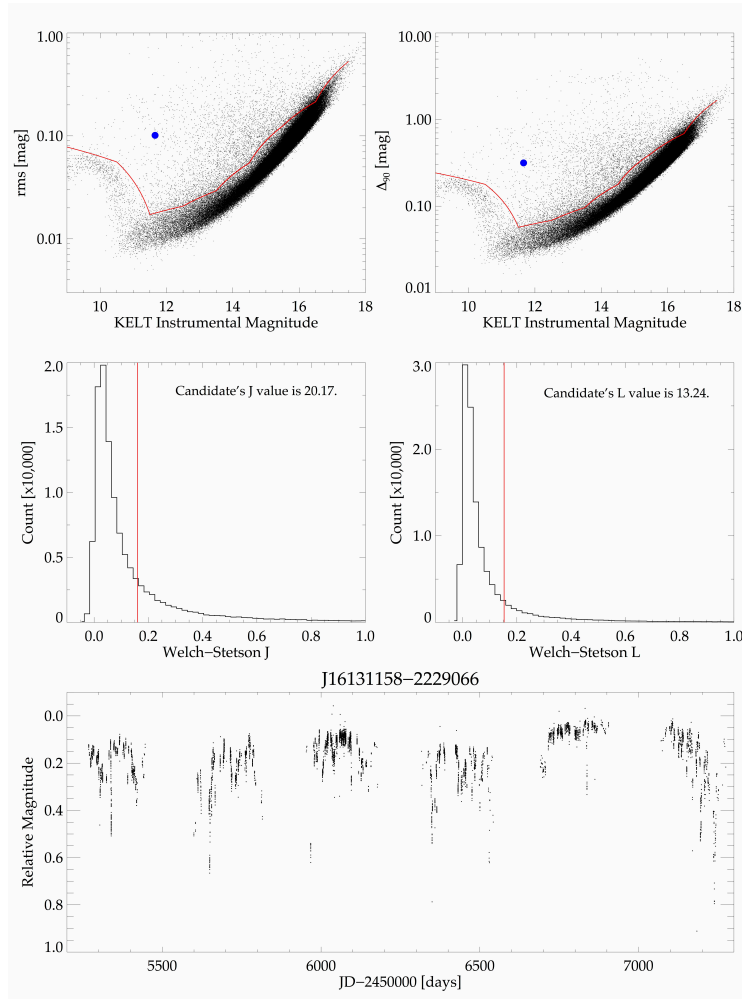


Figure 1. Distributions of the four metrics used to identify variable objects in our sample (see Section 2.3.1). Top panels: rms and Δ_{90} statistics with their respective $+2\sigma$ cuts (red curves) used to identify candidate variables. Middle panels: Welch-Stetson J & L statistics with their respective $+3\sigma$ and $+5\sigma$ cuts (red lines) used to identify candidate variables. Bottom panel: the light curve of an example variable star, J16131158-2229066, whose computed metrics are given in the top (blue points) and middle panels.

3 INTERESTING VARIABLES

3.1 Dippers & UXORs

Four sources in our sample exhibit “dipper” or “UXOR” behavior in their KELT light curves, as shown in Figure 3. Dippers are identified by near-constant maximum brightness levels, punctuated by dimming events that are typically ~ 0.1 – 1.0 mag in depth and last for a couple of days. Dippers are thought to result from occultations of T Tauri stars by circumstellar material orbiting in the inner disk (e.g., Bouvier et al. 1999; Cody et al. 2014; McGinnis et al. 2015; Ansdell et al. 2016b; Bodman et al. 2016). UXOR variables are typically disk-hosting Herbig Ae stars whose light curves also exhibit dimming events, though the events tend to be deeper (~ 1 – 2 mag) and last longer (i.e., weeks to months; Waters & Waelkens 1998; Dullemond et al. 2003) compared to dippers. It is unclear whether dipper and UXOR variability are produced by the same physical mechanism(s), although both classes of objects are thought to be related to transiting circumstellar dust. Indeed, all four of the dipper/UXOR candidates host disks (based on WISE excess), but interestingly

cover a range of disk types (full, transitional, debris; Luhman & Mamajek 2012). Three of these variables (J15554883-2512240, J16131158-2229066, J16141107-2305362) are newly identified with KELT data, while one dipper (J16042165-2130284) was previously identified in $K2/C2$ data (Ansdell et al. 2016a). Each source is discussed below.

J15554883-2512240 exhibits aperiodic dimming events ≈ 0.1 mag in depth, superposed on a periodic signal of 3.72 days, in all six KELT-South seasons. The star also maintains a near-constant maximum brightness level of ≈ 12.7 mag until the last KELT season, during which it steadily dims by ≈ 0.1 mag. Interestingly, the source does not exhibit dipper behavior in its $K2/C2$ light curve, although dippers are known to change their behavior over time (e.g., McGinnis et al. 2015; Ansdell et al. 2016b). The star has a G3V spectral type and hosts a “debris/evolved transitional” disk (Luhman & Mamajek 2012). This disk was not detected in a sub-mm ALMA survey of Upper Sco (Barenfeld et al. 2016) and the disk inclination remains unknown.

J16042165-2130284 and J16042097-2130415 are blended in both their KELT and $K2/C2$ images, with their

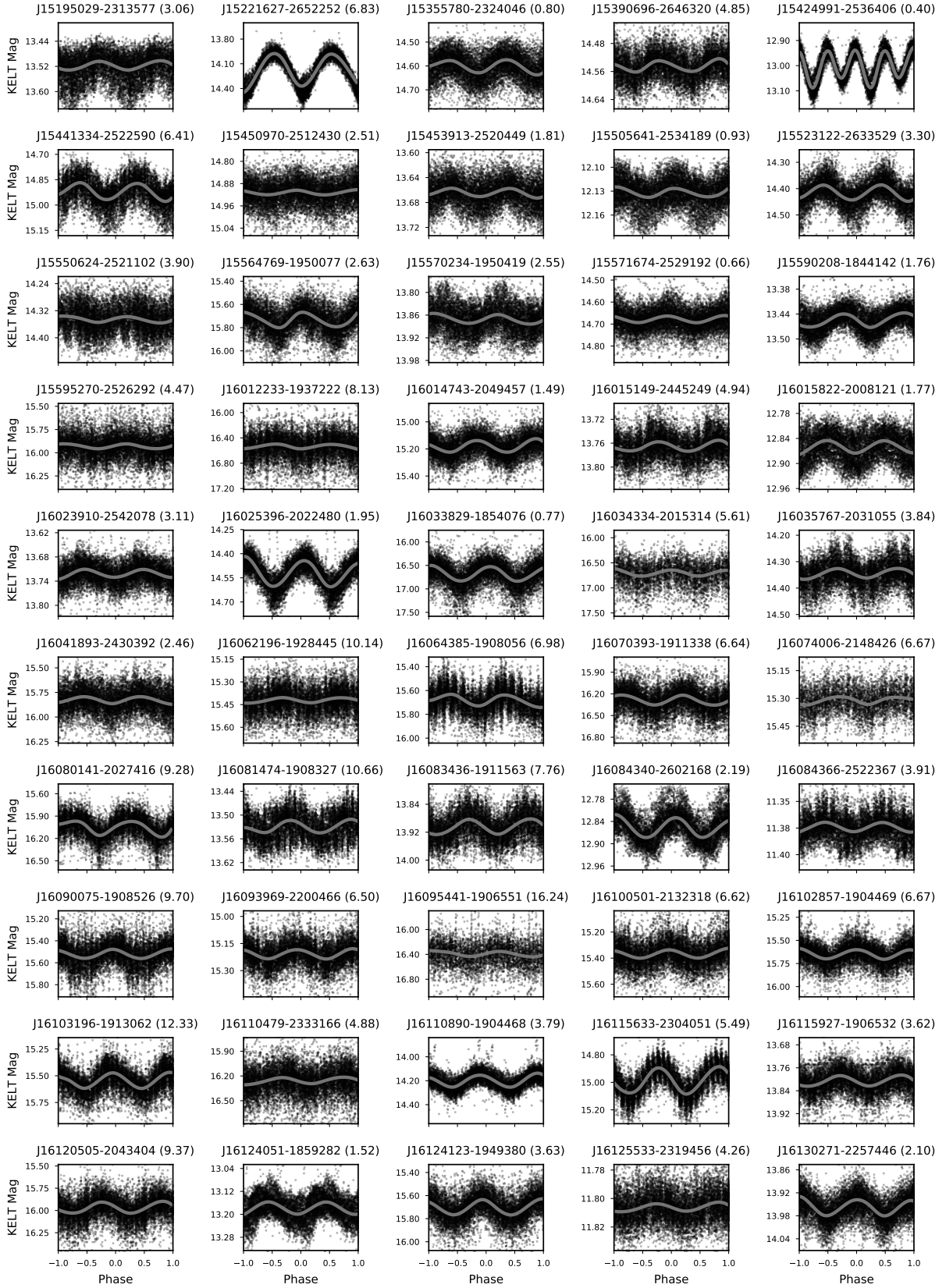


Figure 2. Phase-folded KELT light curves (replicated over two full phases) for the sources in our sample exhibiting periodic signals (see Section 2.3.2). Smoothed medians are shown by the gray lines and the source 2MASS names are given at the top of each panel along with the derived rotation periods (in days) in parentheses. We do not show sources with potentially blended KELT light curves (flagged in Table 1) or the more exotic variables described in Section 3 (see instead Figures 3 and 4).

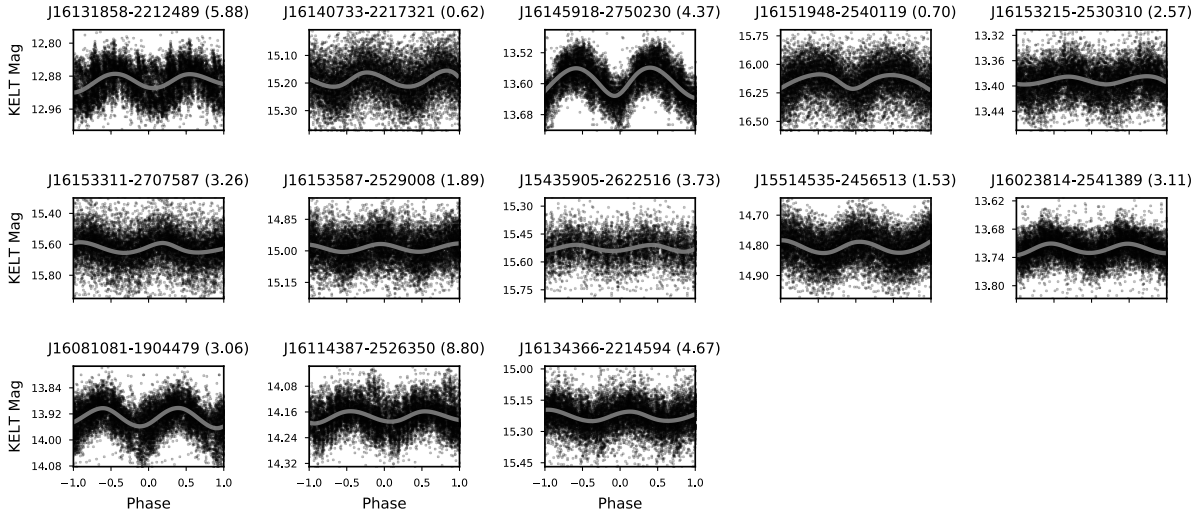


Figure 2 (Cont.).

combined light curves exhibiting dipper behavior in both datasets. However, because the sources have a sufficiently large projected separation ($\approx 16''$), Ansdell et al. (2016a) were able to manually extract their individual $K2/C2$ light curves from the *Kepler* Target Pixel File using custom photometric apertures. They found that J16042165-2130284 is the source of the dipper behavior, with J16042097-2130415 contributing little to the photometric variability. Indeed, J16042097-2130415 does not appear to host a disk based on its lack of infrared excess in WISE pass-bands (Luhman & Mamajek 2012). In contrast, J16042165-2130284 has a K2V spectral type and hosts a well-characterized face-on transition disk (Mathews et al. 2012; Zhang et al. 2014). The system, which is also known simply as J1604, has a KELT light curve that shows a constant maximum brightness level of ≈ 14.0 mag, punctuated by aperiodic dimming events ≈ 1 mag in depth, and superposed on a 5.10-day periodic signal, consistent with the variability seen in its $K2/C2$ light curve (Ansdell et al. 2016a). The KELT data confirm that this target has been exhibiting dipper-like behavior for at least the last 5.5 years.

J16141107-2305362 exhibits a constant maximum brightness level of ≈ 12.9 mag in its KELT light curve with dimming events ≈ 0.2 mag in depth. The star has a K2V spectral type and hosts a full disk (Luhman & Mamajek 2012), which has also been detected in the sub-mm with ALMA (Carpenter et al. 2014). Its $K2/C2$ light curve shows variable behavior common to young star-disk systems, but is dominated by a 2.8-day periodic signal that is likely the rotation period of the star. The KELT data, however, reveal a longer periodic signal at 35.89 days, which may be related to a stellar activity cycle. This target also has a close stellar companion with a projected separation of 32 AU (Metchev & Hillenbrand 2009).

J16131158-2229066 has a KELT light curve that exhibits aperiodic dimming events ≈ 0.4 mag in depth, superimposed on a varying maximum brightness level with no detectable periodic signal. The star has an A8III/IV spectral type, hosts a full disk, and exhibits clear signatures of ongoing accretion (Luhman & Mamajek 2012). These fea-

tures make J16131158-2229066 more consistent with UXOR variables rather than dippers. Its inner disk also has an inclination of $\approx 60^\circ$ (Lazareff et al. 2017), which may provide the obscuring circumstellar material causing the dimming events. Its $K2/C2$ light curve shows similar variability, but this star was not identified in previous dipper/UXOR searches due to concerns with saturation (Ansdell et al. 2016b). Ripepi et al. (2015) also found high-frequency ($30\text{--}40\text{ d}^{-1}$), low-amplitude (ppt) variability consistent with δ Scuti pulsations using $K2/C2$ short-cadence data. These pulsation signatures are not seen in the KELT data due to the insufficient cadence and sensitivity of the survey.

Three sources in our sample (J16035767-2031055, J16090075-1908526, J16100501-2132318) were previously identified as dippers from their $K2/C2$ light curves (Ansdell et al. 2016b), but are not identified as such by our KELT data. This is likely due to a combination of their optical faintness and moderate dimming, rather than a change in their dipping behavior. J16035767-2031055 is faint ($V = 12.8$) with relatively shallow (0.1 mag) dips in its $K2/C2$ light curve. J16090075-1908526 shows deeper (0.2 mag) dips, but is likely too faint ($V = 13.8$) for KELT to clearly detect this level of variability (although its KELT light curve does show hints of dipper behavior; see Figure 2). Similarly, J16100501-2132318 has extremely shallow (0.03 mag) dips in its $K2/C2$ light curve and is also faint ($V = 13$ mag), making its variability difficult to detect with KELT.

3.2 Long-term Periodicity and Dimming

Three sources in our sample (J15375186-2326574, J15554141-2043150, J16081050-2351024) exhibit periodic signals in their KELT light curves at > 20 days, which is too long to be associated with stellar rotation for young (~ 10 Myr) pre-main sequence (PMS) stars. Six additional sources (J15413121-2520363, J15545986-2347181, J15581270-2328364, J15583692-2257153, J16004056-2200322, J16102888-2213477) show very long-term variability at $\gg 100$ days, which may potentially be cyclic, although longer time baselines are needed to confirm this.

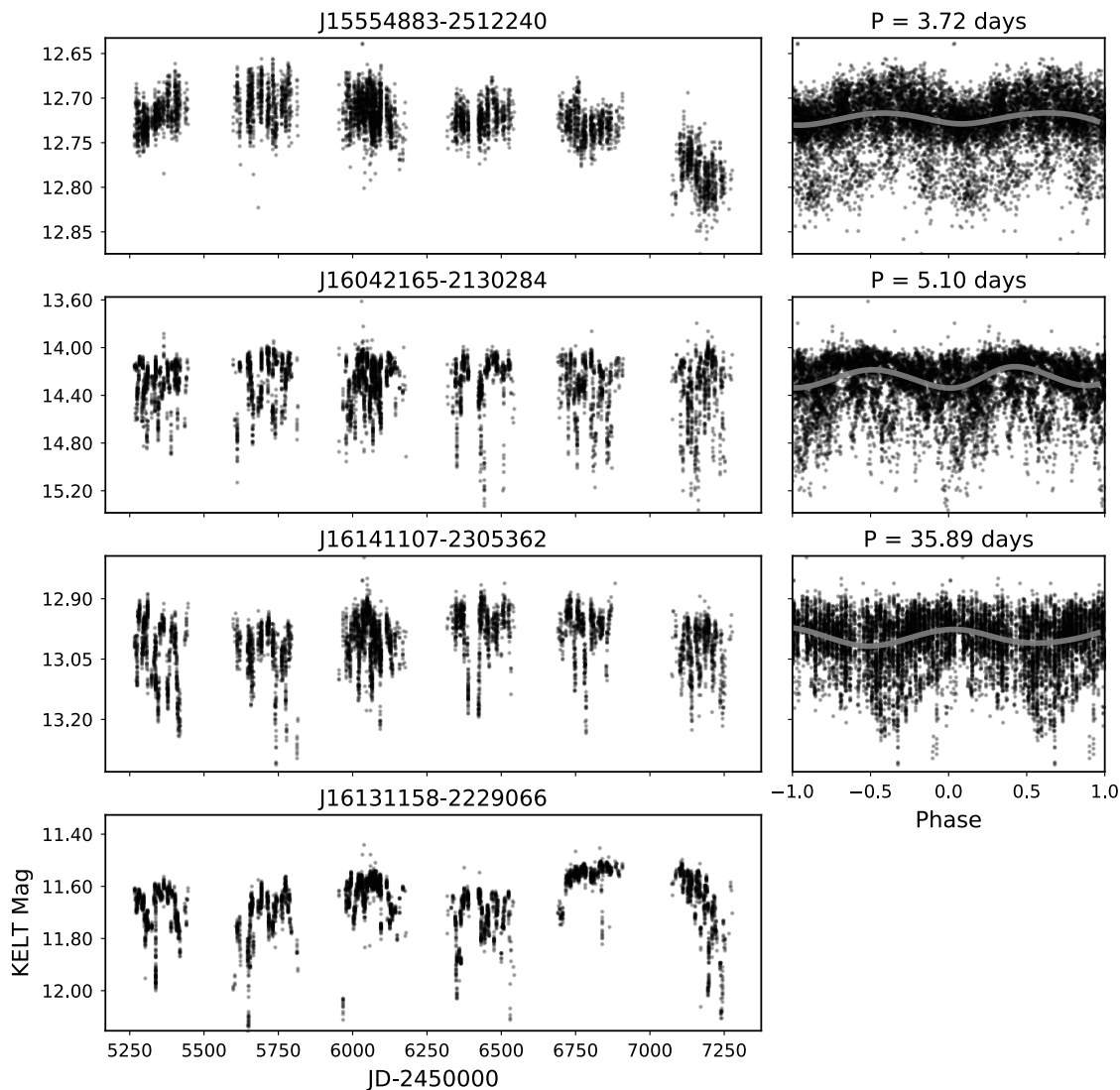


Figure 3. The full KELT light curves (left) for the four dipper/UXOR candidates discussed in Section 3.1; source 2MASS names are given at the top of each panel. Phased light curves (right; replicated over two full phases) are provided for the three sources that also show periodic variability; smoothed medians are shown by the gray lines and derived rotation periods are given at the top of each panel.

These nine sources are discussed below and their light curves are shown in Figure 4. We consider the possibility of their long-term variability being related to stellar activity cycles in Section 4.3.

J16081050-2351024 has an F3 spectral type and hosts a “debris/evolved transitional” disk (Luhman & Mamajek 2012). Its KELT light curve shows a 109-day period and Ripepi et al. (2015) have used its *K2*/C2 light curve to classify the star as a γ Dor variable exhibiting multiple low-amplitude (ppt), high-frequency ($\lesssim 1 \text{ d}^{-1}$) pulsations.

J15554141-2043150 was identified as an Upper Sco member of M1 spectral type by Rizzuto et al. (2015), who found clear lithium absorption ($EW(\text{Li}) = 0.64 \text{ \AA}$) and strong $H\alpha$ emission ($EW(H\alpha) = -6.1 \text{ \AA}$) consistent with a PMS star, though no WISE infrared excess indicative of a disk. The source exhibits a 33-day period in the KELT data and a clear 1-day period in its *K2*/C2 light curve with 10% amplitude.

J15375186-2326574 was identified as a young star of K2V spectral type by Preibisch et al. (1998); however, due

to its weak lithium absorption ($EW(\text{Li}) = 0.12 \text{ \AA}$), they classified it as a candidate young cluster member rather than a PMS star. This source exhibits a 153-day period in our KELT data and will be observed during *K2*/C15. No shorter periods are found in the KELT data.

The six sources showing very long-term variability are all classified as G-type stars. J15413121-2520363 and J16102888-2213477 are classified as active G-type sub-giants (G9IVe and G7IVe, respectively; Torres et al. 2006), though their apparent low surface gravity is likely rather due to their PMS status. Indeed, both the KELT and *K2*/C2 data of J16102888-2213477 contain a 2.29-day periodic signal, which is presumably due to stellar rotation. While no rotation period is found in the KELT data for J15413121-2520363, the star will be observed during *K2*/C15. J15545986-2347181, J16004056-2200322, and J15581270-2328364 all have G dwarf spectral types (G3, G9, and G6, respectively; Torres et al. 2006) with stellar rotation periods found with KELT and *K2*/C2 data of 1.06, 2.71, and 1.72 days, respectively.

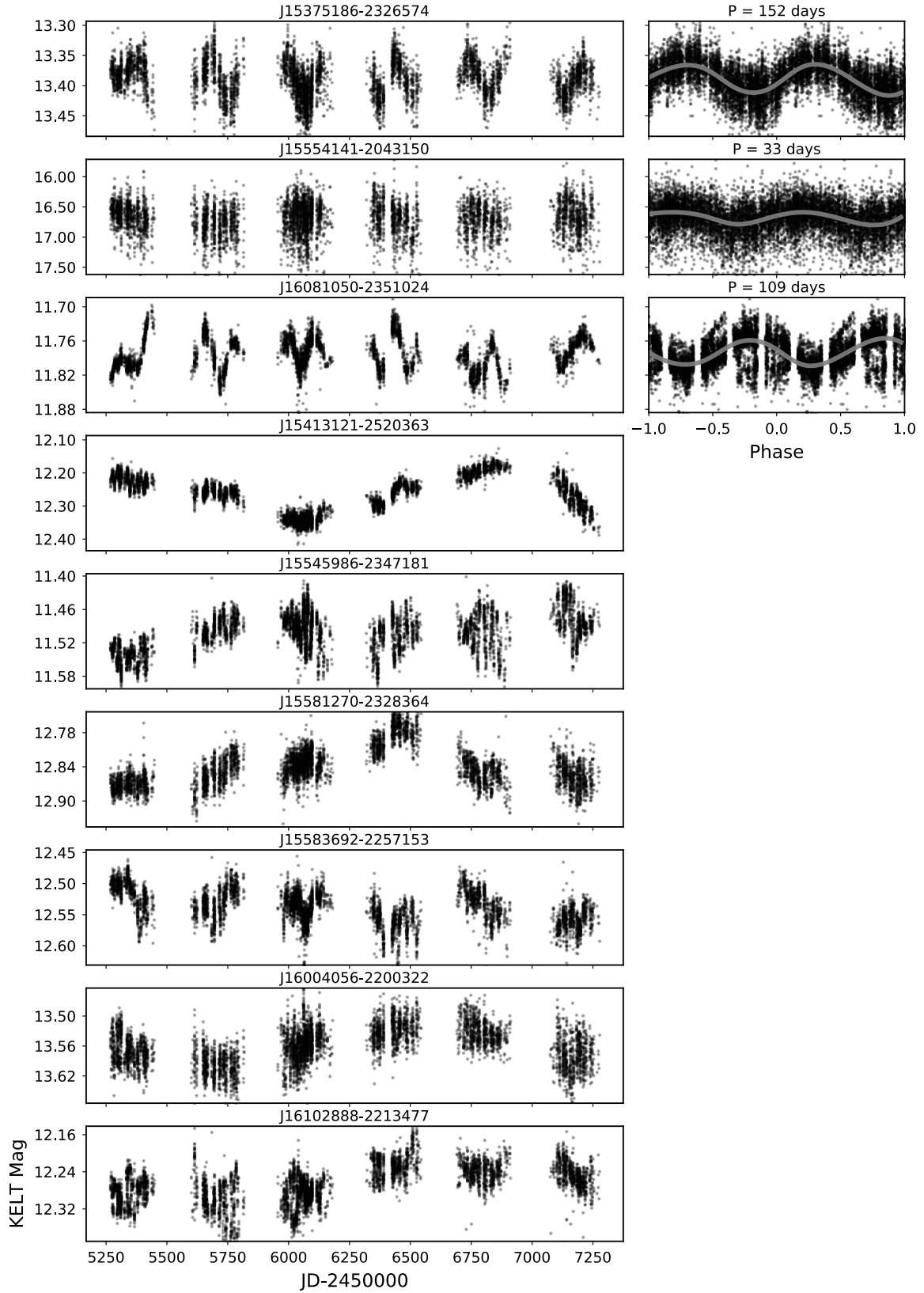


Figure 4. The full KELT light curves (left) for the long-term variables discussed in Section 3.2; source 2MASS names are given at the top of each panel. For those with identifiable periodic signals, we also show their phased light curves (right; replicated over two full phases) with smoothed medians (gray lines); the derived rotation periods are given at the top of each panel .

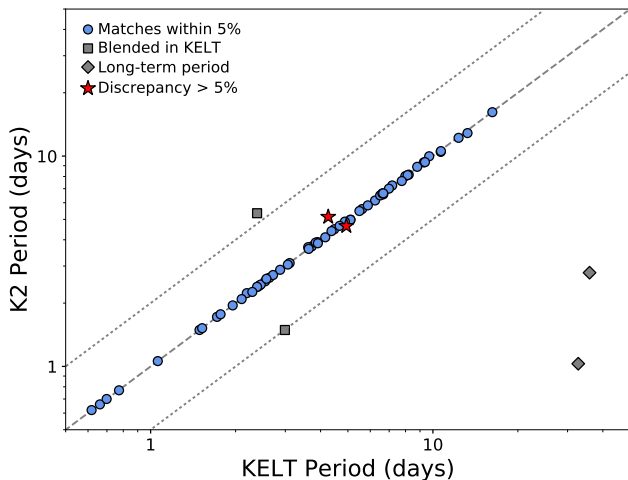


Figure 5. Comparison of the rotational periods identified from KELT and *K2*/C2 data for the 67 sources in our sample for which we could derive significant periodic signals in both datasets (see Section 4.1). The dashed line shows 1:1 agreement, while the dotted lines show the 2 \times and 0.5 \times discrepancies. Only 6 out of the 67 sources are discrepant at > 5% (see Section 4.1 for potential explanations of these discrepant sources).

These sources will all be re-observed in *K2*/C15. Finally, J15583692-2257153 is a G7 star (Luhman & Mamajek 2012) hosting a massive disk with a centrally depleted cavity that has been resolved at sub-mm wavelengths by ALMA (Barenfeld et al. 2016).

4 DISCUSSION

4.1 Comparing KELT and *K2* Periods

In order to test whether the periodic signals found in the KELT data (Section 2.3.2) are indeed stellar rotation periods, we can compare our derived values to the periodic signals found in the *K2*/C2 data, as any true stellar rotation periods should be retrieved in both datasets. To derive periodic signals from the *K2*/C2 data, we apply the LSP to the light curves reduced with the routines of Vanderburg & Johnson (2014), which are made publicly available on the Mikulski Archive for Space Telescopes (MAST).³ We do not apply any rejection criteria for avoiding diurnal or lunar signals (see Section 2.3.2), as these aliases should not occur in the space-based *K2* data. Figure 5 shows the comparison for the 67 targets in our sample for which we could derive periods from both KELT and *K2*/C2 datasets. The periods derived from KELT data match extremely well to those derived from *K2*/C2 data: only six sources are discrepant at > 5% and the median difference is just 0.4%. Thus we can be confident that the periodic signals derived from the KELT data are indeed the stellar rotation periods in the vast majority of cases.

Two of the discrepant sources (J15554141-2043150, J16141107-2305362) have long periods that can be identified

in the long-baseline KELT data (Section 3) but not in the short-baseline *K2*/C2 data. Two other discrepant sources are potential blends: J16082324-1930009 appears to have the period of a brighter nearby star, while J15573430-2321123 shows the 2 \times harmonic of its *K2*/C2 period. The two remaining sources (J16015149-2445249, J16125533-2319456) show only 6% and 20% discrepancies, respectively. J16015149-2445249 has a clear periodic signal in its *K2*/C2 data, but is relatively faint ($V = 12.5$) for KELT, thus the discrepancy may be due to large uncertainty in the derived KELT period. J16125533-2319456 shows a secondary peak in its *K2*/C2 periodogram that is within 10% of the derived KELT period, thus the discrepancy may be due to an unresolved binary.

The excellent match between the periodic signals derived from KELT and *K2*/C2 data also demonstrates that long-term ground-based surveys like KELT are valuable tools for accurately deriving the rotation periods of young stars, so long as the target brightness is within the magnitude range for which the telescope is designed. Indeed, there are only 20 sources in our sample for which periods could be found with *K2*/C2 but not KELT; these are typically too faint for precise photometry with KELT (median $V = 13.7$) or have very low-amplitude variability ($\ll 1\%$).

4.2 Rotational Evolution of PMS Stars

Comparing the distributions of rotation periods for co-eval groups of young stars can inform early stellar evolution. In particular, such a comparison can provide insight into the spin-up of young stars as they contract toward the main sequence, the braking of stellar rotation via magnetized stellar winds that serve to remove angular momentum, and the exchange of angular momentum between the outer layers of stars with their interiors as well as any circumstellar disks (e.g., see the recent review in Gallet & Bouvier 2015). To this end, Figure 6 shows rotation period as a function of absolute 2MASS K_S magnitude (M_K), a proxy for stellar mass, for Upper Sco compared to two older stellar clusters, the Pleiades (125 Myr; Stauffer et al. 1998) and Praesepe (790 Myr; Brandt & Huang 2015).

The rotation periods for Pleiades and Praesepe members are taken from Rebull et al. (2016) and Rebull et al. (2017), respectively, who derived these values from *K2* light curves. For Upper Sco, we estimate rotation periods for 208 candidate members observed during *K2*/C2 by again taking the publicly available light curves reduced using the routines of Vanderburg & Johnson (2014) (see Section 4.1), then identifying significant periods between 0.2 and 30 days using both the LSP and the auto-correlation function (ACF; McQuillan et al. 2013), with the ACF periods given priority. We also take from Table 1 the KELT rotation periods for *K2*/C15 targets that have not yet been observed by *K2*. To calculate M_K we assume distances of 145 pc for Upper Sco, 135 pc for the Pleiades (Melis et al. 2014), and 180 pc for Praesepe (van Leeuwen 2009). We also show in Figure 6 approximate stellar masses, which we derive by comparing M_K to Baraffe et al. (2015) stellar evolution models at the given cluster ages; the x -axis of each plot is scaled to cover the same inferred stellar mass range for all three clusters. The Upper Sco members exhibiting significant excess WISE emission and thus likely hosting circumstellar disks (Luhman & Mamajek 2012) are marked as black points in Figure 6.

³ <https://archive.stsci.edu/k2/hlsp/k2sff/search.php>

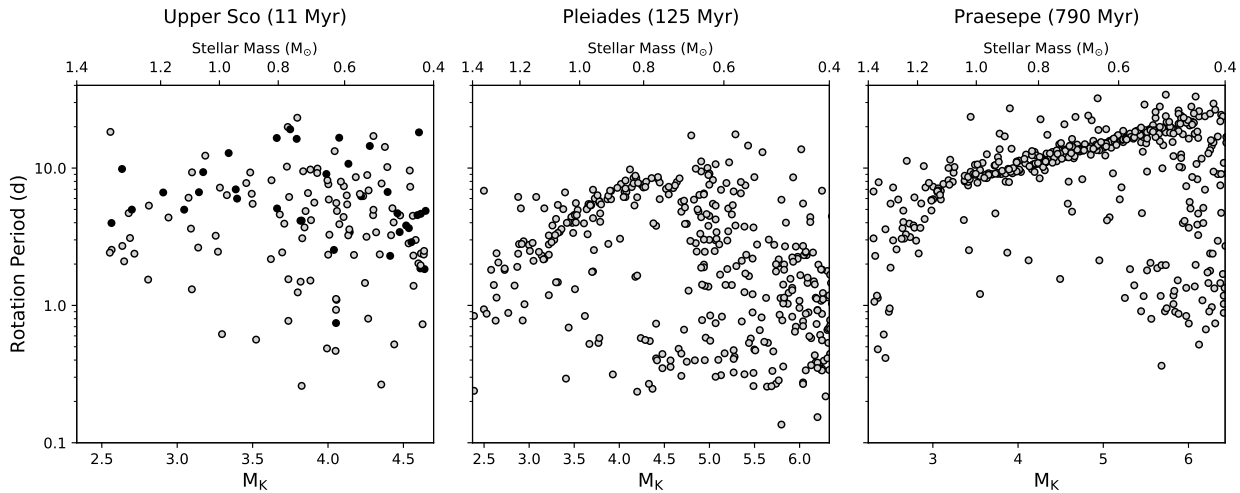


Figure 6. Rotation period as a function of M_K (a proxy for stellar mass) for members Upper Sco (this work), the Pleiades (Rebull et al. 2016), and Praesepe (Rebull et al. 2017). M_K was derived from 2MASS photometry assuming distances of 145 pc for Upper Sco, 125 pc for Pleiades, and 180 pc for Praesepe. Approximate stellar masses are shown on the top axes and derived from Baraffe et al. (2015) isochrones for ages of 10 Myr for Upper Sco, 120 Myr for Pleiades, and 800 Myr for Praesepe. Upper Sco members likely hosting disks (as determined by excess infrared WISE emission) are indicated by black points.

The wide spread in rotation periods seen for Upper Sco members is representative of a classic problem in early stellar evolution studies (e.g., Krishnamurthi et al. 1997). As young stars contract toward the main sequence, conservation of angular momentum dictates that spin rates increase. However, other mechanisms also influence stellar rotation rates, in particular disk-star “locking” via magnetic torquing as well as “braking” via magnetized stellar winds (e.g., Landin et al. 2016). These competing mechanisms, in addition to differences in initial angular momenta, likely result in the large dispersion in rotation periods seen at the young (≈ 5 –11 Myr) age of Upper Sco. However, Figure 6 also shows the well-known evolution from this broad distribution of rotation periods to a tightly converged sequence that is clearly apparent by the age of the Pleiades (125 Myr) for $M_{\star} \gtrsim 0.7 M_{\odot}$, and extends down to low-mass stars ($M_{\star} \gtrsim 0.4 M_{\odot}$) by the age of Praesepe (790 Myr).

Given that most cool Upper Sco members still have faster rotation periods compared to stars along the loci seen in Praesepe, angular momentum loss via magnetized winds must be important at ages beyond that of Upper Sco; disk-star locking is unlikely to play a major role in spin-down, as only about 7% of Upper Sco members are currently accreting (Pecaut & Mamajek 2016), meaning that any disk-locking is *fait accompli* (barring star formation within the past few Myr). Figure 6 also suggests that even at the young age of Upper Sco, stars more massive than $\approx 0.8 M_{\odot}$ may be beginning to converge toward the loci seen at older ages. Lower-mass stars that are still evolving toward the main sequence will resist spin-down due to their more massive convective envelopes and higher moments of inertia (when “unlocked” from the disk, and assuming that the inner radiative core and outer convective envelope of a star are only weakly coupled). This could explain the progressive disappearance of the dispersion of rotation periods as a function of stellar mass seen in Figure 6. Reality may be more complex, however, since the h Persei region at 13 Myr shows no decline

in the dispersion of rotation period with stellar mass (see Figure 11 in Moraux et al. 2013).

We also note that the distribution of rotation periods for Upper Sco members has an envelope with an upper edge of ≈ 10 –20 days for low-mass ($\lesssim 0.8 M_{\odot}$) stars, decreasing to shorter periods for higher-mass stars. A similar distribution was found for Upper Sco in the ground-based SuperWASP data analyzed in Mellon et al. (2017), although with an upper bound of 8 days (see also Scholz et al. 2015 for an extension to the brown dwarf regime at $M_K > 8$). The longer-period signals seen here could be produced by binaries as well as older interloping stars, although many of the longer-period stars in Upper Sco appear to host disks, suggesting that they are indeed young ($\lesssim 10$ Myr).

4.3 Stellar Activity Cycles

Ten sources in our sample showed long-term (> 20 -day) variability in their KELT light curves (see Sections 3.1 & 3.2). Four of these sources exhibited clear periodic signals, which are too long to be explained by stellar rotation for ~ 10 Myr old PMS stars. The other six sources showed hints of much longer-term (100s of days) cyclic behavior, which may become clearer with longer-baseline observations.

Such long-term variability may be related to solar-like magnetic activity cycles that drive significant changes in spot coverage over time, which in turn modulate the brightness variations observed by KELT. Indeed, these long-term variables are strongly biased toward G-type and early K-type sources compared to the rest of our sample. Moreover, only two of these sources (J15583692-2257153, J16141107-2305362) host full disks, thus the long-term variability is unlikely to be solely due to cyclic changes in the interaction between the inner disk and the stellar magnetic field, which has been previously suggested to explain long-term periods seen in WASP data of T Tauri stars (Rigon et al. 2017).

5 SUMMARY

We presented and analyzed light curves spanning 5.5 years from the ground-based KELT survey for 131 candidate members of Upper Sco that are also targets of the *K2* mission. The long-baseline KELT data published in this paper (available online as electronic tables) provide a legacy dataset that complements the much higher-precision but shorter-duration photometric observations from *K2*, thereby enabling more complete studies of young star variability.

In our analysis, we found periodic signals for 89 stars in our sample, the vast majority of which are consistent with the rotation of spots on the surface of young stars. Namely, the periods span ~ 0.5 –10 days and have amplitudes of a few percent. We also identified stars exhibiting interesting variability apart from stellar rotation. In particular, we identified four sources exhibiting dipper/UXOR behavior, which is thought to be due to occultations of stars by dusty circumstellar material. The KELT data were able to identify new dippers and, when combined with *K2*/C2 data, also confirm long-term dipper behavior as well as the disappearance of dipper-like variability. Ten sources also showed potentially long-term cyclic behavior, which we interpreted as possibly being related to solar-like cycles of magnetic activity.

We also compared the periodic signals derived from KELT data to those derived from *K2*/C2 data for 67 sources. The excellent agreement confirmed that these periodic signals are likely stellar rotational signals, and also illustrated the power of long-term ground-based surveys for accurately deriving the rotation periods of young stars. Additionally, we compared the distribution of rotation period versus stellar mass in Upper Sco to those of the older Pleiades and Praesepe regions in order to analyze the angular momentum evolution of young stars from ≈ 10 –800 Myr.

The continuation of long-term ground-based photometric monitoring surveys like KELT will be important for putting into context the high-precision data obtained from space-based missions beyond *K2*. In particular, the upcoming *Transiting Exoplanet Survey Satellite* (*TESS*; Ricker et al. 2014) mission will obtain high-precision photometric observations of almost the entire sky for a duration of $\gtrsim 27$ days. When *TESS* is in operation, KELT can provide $\gtrsim 10$ years of complementary long-baseline data for studying the underlying processes driving young star variability and their relation to planet formation.

ACKNOWLEDGEMENTS

Early work on KELT-North was supported by NASA Grant NNG04GO70G. J.E.R. was supported by the Harvard Future Faculty Leaders Postdoctoral fellowship. G.S. acknowledges the support of the Vanderbilt Office of the Provost through the Vanderbilt Initiative in Data-intensive Astrophysics (VIDA) fellowship. This work has made use of NASA’s Astrophysics Data System and the SIMBAD database operated at CDS, Strasbourg, France. This document does not contain export controlled information and is under review for Unlimited External Release (URS268385). Part of the research was carried out at the Jet Propulsion Laboratory, California Institute of Technology, under a contract with the National Aeronautics and Space Administration.

REFERENCES

- Ansdell M., Gaidos E., Williams J. P., Kennedy G., Wyatt M. C., LaCourse D. M., Jacobs T. L., Mann A. W., 2016a, *MNRAS*, **462**, L101
- Ansdell M., et al., 2016b, *ApJ*, **816**, 69
- Baglin A., et al., 2006, in 36th COSPAR Scientific Assembly.
- Baraffe I., Homeier D., Allard F., Chabrier G., 2015, *A&A*, **577**, A42
- Barenfeld S. A., Carpenter J. M., Ricci L., Isella A., 2016, *ApJ*, **827**, 142
- Bertout C., 1989, *ARA&A*, **27**, 351
- Bodman E. H. L., et al., 2016, preprint, ([arXiv:1605.03985](https://arxiv.org/abs/1605.03985))
- Borucki W. J., et al., 2010, *Science*, **327**, 977
- Bouvier J., et al., 1999, *A&A*, **349**, 619
- Brandt T. D., Huang C. X., 2015, *ApJ*, **807**, 24
- Burger D., Stassun K. G., Pepper J., Siverd R. J., Paegert M., De Lee N. M., Robinson W. H., 2013, *Astronomy and Computing*, **2**, 40
- Carpenter J. M., Mamajek E. E., Hillenbrand L. A., Meyer M. R., 2006, *ApJ*, **651**, L49
- Carpenter J. M., Ricci L., Isella A., 2014, *ApJ*, **787**, 42
- Cody A. M., et al., 2014, *AJ*, **147**, 82
- Cody A. M., Hillenbrand L. A., David T. J., Carpenter J. M., Everett M. E., Howell S. B., 2017, *ApJ*, **836**, 41
- Drake A. J., et al., 2009, *ApJ*, **696**, 870
- Dullemond C. P., van den Ancker M. E., Acke B., van Boekel R., 2003, *ApJ*, **594**, L47
- Fazio G. G., et al., 2004, *ApJS*, **154**, 10
- Gallet F., Bouvier J., 2015, *A&A*, **577**, A98
- Henderson C. B., Stassun K. G., 2012, *ApJ*, **747**, 51
- Herbst W., Eislöffel J., Mundt R., Scholz A., 2007, *Protostars and Planets V*, pp 297–311
- Howell S. B., et al., 2014, *PASP*, **126**, 398
- Kraus A. L., Ireland M. J., Martinache F., Lloyd J. P., 2008, *ApJ*, **679**, 762
- Krishnamurthi A., Pinsonneault M. H., Barnes S., Sofia S., 1997, *ApJ*, **480**, 303
- Kuhn R. B., et al., 2016, *MNRAS*, **459**, 4281
- Lafrenière D., Jayawardhana R., van Kerkwijk M. H., Brandeker A., Janson M., 2014, *ApJ*, **785**, 47
- Landin N. R., Mendes L. T. S., Vaz L. P. R., Alencar S. H. P., 2016, *A&A*, **586**, A96
- Lazareff B., et al., 2017, *A&A*, **599**, A85
- Lomb N. R., 1976, *Ap&SS*, **39**, 447
- Luhman K. L., Mamajek E. E., 2012, *ApJ*, **758**, 31
- Mathews G. S., Williams J. P., Ménard F., 2012, *ApJ*, **753**, 59
- McGinnis P. T., et al., 2015, *A&A*, **577**, A11
- McQuillan A., Aigrain S., Mazeh T., 2013, *MNRAS*, **432**, 1203
- Melis C., Reid M. J., Mioduszewski A. J., Stauffer J. R., Bower G. C., 2014, *Science*, **345**, 1029
- Mellon S. N., Mamajek E. E., Oberst T. E., Pecaute M. J., 2017, preprint, ([arXiv:1706.06105](https://arxiv.org/abs/1706.06105))
- Metchev S. A., Hillenbrand L. A., 2009, *ApJS*, **181**, 62
- Morau E., et al., 2013, *A&A*, **560**, A13
- Oelkers R. J., et al., 2015, *AJ*, **149**, 50
- Pecaute M. J., Mamajek E. E., 2016, *MNRAS*, **461**, 794
- Pecaute M. J., Mamajek E. E., Bubar E. J., 2012, *ApJ*, **746**, 154
- Pepper J., et al., 2007, *PASP*, **119**, 923
- Pepper J., Kuhn R. B., Siverd R., James D., Stassun K., 2012, *PASP*, **124**, 230
- Pojmanski G., 1997, *Acta Astronomica*, **47**, 467
- Pollacco D. L., et al., 2006, *PASP*, **118**, 1407
- Preibisch T., Guenther E., Zinnecker H., Sterzik M., Frink S., Roeser S., 1998, *A&A*, **333**, 619
- Preibisch T., Brown A. G. A., Bridges T., Guenther E., Zinnecker H., 2002, *AJ*, **124**, 404
- Rebull L. M., et al., 2016, *AJ*, **152**, 114

- Rebull L. M., Stauffer J. R., Hillenbrand L. A., Cody A. M., Bouvier J., Soderblom D. R., Pinsonneault M., Hebb L., 2017, *ApJ*, **839**, 92
- Ricker G. R., et al., 2014, in *Space Telescopes and Instrumentation 2014: Optical, Infrared, and Millimeter Wave*. p. 914320 ([arXiv:1406.0151](#)), doi:10.1117/12.2063489
- Rigon L., Scholz A., Anderson D., West R., 2017, *MNRAS*, **465**, 3889
- Ripepi V., Balona L., Catanzaro G., Marconi M., Palla F., Giarusso M., 2015, *MNRAS*, **454**, 2606
- Rizzuto A. C., Ireland M. J., Kraus A. L., 2015, *MNRAS*, **448**, 2737
- Rodriguez J. E., et al., 2017a, preprint, ([arXiv:1703.02522](#))
- Rodriguez J. E., et al., 2017b, *ApJ*, **836**, 209
- Scargle J. D., 1982, *ApJ*, **263**, 835
- Scaringi S., et al., 2016, *MNRAS*, **463**, 2265
- Scholz A., Kostov V., Jayawardhana R., Muzić K., 2015, *ApJ*, **809**, L29
- Siverv R. J., et al., 2012, *ApJ*, **761**, 123
- Skrutskie M. F., et al., 2006, *AJ*, **131**, 1163
- Stauffer J. R., Schultz G., Kirkpatrick J. D., 1998, *ApJ*, **499**, L199
- Stauffer J., et al., 2017, *AJ*, **153**, 152
- Stetson P. B., 1996, *PASP*, **108**, 851
- Torres C. A. O., Quast G. R., da Silva L., de La Reza R., Melo C. H. F., Sterzik M., 2006, *A&A*, **460**, 695
- Vanderburg A., Johnson J. A., 2014, *PASP*, **126**, 948
- Wang L., et al., 2013, *AJ*, **146**, 139
- Waters L. B. F. M., Waelkens C., 1998, *ARA&A*, **36**, 233
- Williams J. P., Cieza L. A., 2011, *ARA&A*, **49**, 67
- Zhang K., Isella A., Carpenter J. M., Blake G. A., 2014, *ApJ*, **791**, 42
- Zhang K., Crockett N., Salyk C., Pontoppidan K., Turner N. J., Carpenter J. M., Blake G. A., 2015, *ApJ*, **805**, 55
- de Zeeuw P. T., Hoogerwerf R., de Bruijne J. H. J., Brown A. G. A., Blaauw A., 1999, *AJ*, **117**, 354
- van Leeuwen F., 2009, *A&A*, **497**, 209

Table 1: Upper Sco Members Observed by KELT and *K2*

2MASS ID	EPIC ID	Field	RA _{J2000}	Dec _{J2000}	SpT	Disk	V	K _S	RMS	Var	Blend	Period	Classification	Ref ^f
J15195029-2313577	249386734	15	15:19:50.299	-23:13:57.00	K4	0	10.96	8.86	1.00	1	0	3.0611	Periodic	(4)
J15221627-2652252		15	15:22:16.202	-26:52:23.98	K6	0	11.86	8.66	1.00	1	0	6.8304	Periodic	(4)
J15313976-2520440	249225380	15	15:31:39.698	-25:20:44.01	G9	0	13.21	11.16	0.00	0	0			(4)
J15331002-2323185	249374906	15	15:33:10.000	-23:23:17.98	G9	0	12.49	10.98	0.00	0	0			(4)
J15344110-2322161	249376234	15	15:34:41.100	-23:22:15.99	G5	0	11.48	10.33	0.00	0	0			(4)
J15355780-2324046	249373956	15	15:35:57.796	-23:24:03.99	K3	0	12.21	9.43	0.00	0	0	0.8030	Periodic	(1)
J15375186-2326574	249370343	15	15:37:51.801	-23:26:57.98	K2	0	11.04	7.56	1.00	1	0	152.2776	Periodic/Long-term	(4)
J15381253-2326096	249371327	15	15:38:12.499	-23:26:09.99	K3	0	10.76	8.98	0.00	0	0			(4)
J15390696-2646320	249112324	15	15:39:06.957	-26:46:32.08	M0.5	0	12.78	8.67	0.00	0	0	4.8531	Periodic	(2)
J15413121-2520363	249225568	15	15:41:31.212	-25:20:36.31	G9IVe	0	9.95	7.24	1.00	1	0		Long-term	(1)
J15424991-2536406 [‡]	249205008	15	15:42:49.898	-25:36:38.98	G5	0	10.79	8.18	1.00	1	0	0.3994	Periodic	(3)
J15435905-2622516	249144433	15	15:43:59.064	-26:22:51.60	K9Ve	0	14.07	9.83	0.00	0	0	3.7295	Periodic	(3)
J15441334-2522590	249222494	15	15:44:13.300	-25:22:58.00	M1	0	13.47	9.08	0.00	0	0	6.4121	Periodic	(1)
J15450970-2512430	249235696	15	15:45:09.708	-25:12:42.98	M1.5	0	13.52	9.72	0.00	0	0	2.5117	Periodic	(2)
J15453913-2520449	249225361	15	15:45:39.100	-25:20:44.98	G3	0	11.43	9.13	0.00	0	0	1.8087	Periodic	(4)
J15465590-2016022	249619259	15	15:46:55.898	-20:16:01.99	G0	0	11.40	10.16	0.00	0	0			(4)
J15492100-2600062	249174457	15	15:49:21.000	-26:00:06.30	K0.5	0	11.00	7.91	1.00	1	0			(1)
J15492289-2606068	249166617	15	15:49:22.800	-26:06:06.98	G1	0	12.04	10.08	0.00	0	0			(4)
J15495979-2509033	249240256	15	15:49:59.786	-25:09:03.56	A2V	1	9.25	7.89	0.00	0	0			(1)
J15505641-2534189	203604834	15	15:50:56.419	-25:34:18.98	G0	0	9.75	7.91	0.00	0	0	0.9265	Periodic	(1)
J15514535-2456513	203782856	15	15:51:45.360	-24:56:51.36	K3IV	0	12.37	9.53	0.00	0	0	1.5284	Periodic	(3)
J15523122-2633529	203307585	15	15:52:31.226	-26:33:52.95	M0	0	12.31	8.98	0.00	0	0	3.3018	Periodic	(1)
J15545986-2347181	204069863	02/15	15:54:59.868	-23:47:18.16	G3V	0	9.01	7.03	1.00	1	1	1.0601	Periodic/Long-term	(1)
J15550213-2149434	204562176	02/15	15:55:02.140	-21:49:43.50	M0.0	0	12.25	8.64	0.00	0	1	4.1558	Periodic	(2)
J15550624-2521102	203667805	02	15:55:06.242	-25:21:10.22	M1	0	12.57	8.51	0.00	0	0	3.9047	Periodic	(1)
J15551704-2322165	204174563	02/15	15:55:17.040	-23:22:16.60	M2.5	1	13.85	9.33	0.00	0	1			(1)
J15551758-2322036	204175508	02/15	15:55:17.584	-23:22:03.75	A4IV/V	0	8.43	7.39	0.00	0	1			(1)
J15552980-2544499	203553934	02	15:55:29.812	-25:44:49.99	M0.5	0	13.43	9.14	0.00	0	0			(2)
J15554141-2043150	204819202	02	15:55:41.412	-20:43:15.09	M1.0	0	13.78	9.45	0.00	0	0	32.7250	Periodic/Long-term	(2)
J15554883-2512240	203710077	02	15:55:48.835	-25:12:24.08	G3V	1	10.50	8.29	1.00	1	0	3.7226	Periodic/Dipper	(1)
J15562941-2348197	204065688	02/15	15:56:29.400	-23:48:19.00	M1.5	0	12.79	8.74	0.00	0	1	7.9855	Periodic	(1)
J15563719-2332012	204133258	02/15	15:56:37.200	-23:32:00.99	G1	0	12.17	10.61	0.00	0	1			(4)
J15564769-1950077	205010817	02	15:56:47.690	-19:50:07.62	M2.0	0	13.37	8.95	0.00	0	0	2.6345	Periodic	(2)
J15565545-2258403	204274993	02/15	15:56:55.461	-22:58:40.40	M0	0	13.42	9.43	0.00	0	1	8.2100	Periodic	(1)
J15570234-1950419	205008763	02	15:57:02.299	-19:50:40.99	K7	0	11.70	8.37	0.00	0	0	2.5458	Periodic	(1)
J15571674-2529192 [‡]	203628765	02	15:57:16.740	-25:29:19.32	M0	0	12.54	8.86	0.00	0	0	0.6612		(1)
J15571998-2338499	204104882	02/15	15:57:19.987	-23:38:49.99	M0	0	12.65	8.88	0.00	0	1	6.2388	Periodic	(1)
J15572575-2354220	204040060	02/15	15:57:25.759	-23:54:21.99	M0.5	0	13.50	9.09	0.00	0	1	7.1756	Periodic	(1)
J15573430-2321123	204179058	02/15	15:57:34.310	-23:21:12.31	M1	1	13.12	8.99	0.00	0	1	2.9901	Periodic	(2)
J15581270-2328364	204147776	02/15	15:58:12.698	-23:28:36.40	G6	1	10.37	8.02	1.00	1	1	1.7185	Periodic/Long-term	(1)
J15582965-2441445	203850326	02	15:58:29.599	-24:41:43.98	G0	0	13.22	11.70	0.00	0	0			(4)
J15583692-2257153	204281213	02/15	15:58:36.921	-22:57:15.33	G7	1	10.15	7.05	1.00	1	1		Long-term	(1)
J15590208-1844142	205230905	02	15:59:02.001	-18:44:13.99	K6.5	0	11.94	8.11	0.00	0	0	1.7647	Periodic	(1)

Table 1: continued

J15595270-2526292	203642381	02	15:59:52.689	-25:26:29.18	M0.5	0	13.47	9.72	0.00	0	0	4.4724	Periodic	(2)
J16004056-2200322	204519031	02/15	16:00:40.560	-22:00:32.18	G9	0	10.88	8.44	1.00	1	1	2.7147	Periodic/Long-term	(1)
J16010519-2227311	204406748	02/15	16:01:05.193	-22:27:31.17	M3	0	13.11	8.75	0.00	0	1			(1)
J16012233-1937222	205055104	02	16:01:22.336	-19:37:22.29	M1.5	0	14.14	9.56	0.00	0	0	8.1341	Periodic	(2)
J16012563-2240403	204350686	02/15	16:01:25.624	-22:40:40.33	K3	0	13.41	8.52	1.00	1	1	2.3918	Periodic	(1)
J16014743-2049457	204794876	02	16:01:47.400	-20:49:45.01	M0	0	13.10	8.61	0.00	0	0	1.4900	Periodic	(1)
J16015149-2445249	203834337	02	16:01:51.492	-24:45:24.94	K7	0	12.48	8.48	0.00	0	0	4.9359	Periodic	(1)
J16015790-2100353	204754061	02	16:01:57.897	-21:00:34.99	G2	0	11.36	9.76	0.00	0	0			(4)
J16015822-2008121	204947015	02	16:01:58.224	-20:08:12.15	G7	0	10.45	7.67	1.00	1	0	1.7692	Periodic	(1)
J16020039-2221237	204432860	02/15	16:02:00.388	-22:21:23.90	M1	1	13.12	8.84	0.00	0	1	2.8761	Periodic	(1)
J16020845-2254588	204290833	02/15	16:02:08.450	-22:54:59.11	M1	0	13.59	9.55	0.00	0	1			(1)
J16021045-2241280	204347304	02/15	16:02:10.500	-22:41:29.00	K6	0	11.61	8.06	0.00	0	1			(1)
J16023814-2541389	203569230	02	16:02:38.136	-25:41:39.12	K8IVe	0	13.05	9.33	0.00	0	0	3.1083	Periodic	(3)
J16023910-2542078	203566940	02	16:02:39.096	-25:42:06.98	K7	0	12.17	9.12	0.00	0	0	3.1083	Periodic	(1)
J16025123-2401574	204008342	15	16:02:51.199	-24:01:55.99	K4	1	12.12	8.93	0.00	0	1	3.5112	Periodic	(1)
J16025243-2402226	204006744	15	16:02:52.399	-24:02:21.98	K0	0	11.43	7.64	0.00	0	1	3.5112	Periodic	(1)
J16025396-2022480 [‡]	204894575	02	16:02:53.959	-20:22:48.07	K6	0	12.70	8.19	1.00	1	0	1.9531	Periodic	(1)
J16033550-2245560	204328600	02/15	16:03:35.500	-22:45:56.08	K0	0	11.13	8.36	1.00	1	1	2.4253	Periodic	(1)
J16033829-1854076	205199316	02	16:03:38.299	-18:54:07.70	M1.0	0	14.36	9.54	0.00	0	0	0.7728	Periodic	(2)
J16034187-2005577	204954915	02	16:03:41.870	-20:05:57.69	M2	0	14.03	9.49	0.00	0	0			(1)
J16034334-2015314	204920926	02	16:03:43.339	-20:15:31.39	M2	0	14.18	9.72	0.00	0	0	5.6130	Periodic	(1)
J16034695-2245246 [‡]	204330803	02/15	16:03:46.951	-22:45:24.69	M1.5	0	13.38	9.10	0.00	0	1	13.2620	Periodic	(2)
J16035767-2031055	204864076	02	16:03:57.600	-20:31:05.01	K5	1	12.87	8.37	1.00	1	0	3.8443	Periodic	(1)
J16041893-2430392	203895983	02	16:04:18.933	-24:30:39.31	M2.5	1	13.47	8.85	0.00	0	0	2.4552	Periodic	(2)
J16042097-2130415	204637622	02	16:04:20.973	-21:30:41.54	M3.5	0	14.28	9.43	1.00	1	1	5.1043	Periodic/Dipper	(1)
J16042165-2130284	204638512	02	16:04:21.700	-21:30:28.00	K2	1	12.26	8.51	1.00	1	1	5.1043	Periodic/Dipper	(1)
J16062196-1928445	205084870	02	16:06:22.048	-19:28:44.50	M0.5	1	13.34	8.62	0.00	0	0	10.1389	Periodic	(1)
J16064385-1908056	205154017	02	16:06:43.864	-19:08:05.49	K6	1	13.55	9.20	0.00	0	0	6.9845	Periodic	(1)
J16070356-2036264	204844509	02	16:07:03.561	-20:36:26.49	M0	0	12.38	8.10	1.00	1	0			(1)
J16070393-1911338	205142483	02	16:07:03.900	-19:11:31.99	M1	0	13.97	9.22	0.00	0	0	6.6376	Periodic	(1)
J16071778-2203364	204506777	02	16:07:17.788	-22:03:36.46	F8V	0	8.74	7.05	0.00	0	0			(1)
J16074006-2148426	204566199	02	16:07:40.058	-21:48:42.69	M0.5	0	13.21	9.67	0.00	0	0	6.6721	Periodic	(2)
J16074449-2036030	204845955	02	16:07:44.493	-20:36:03.06	M4	0	14.35	9.08	0.00	0	0			(1)
J16080141-2027416	204876697	02	16:08:01.420	-20:27:41.68	K8	0	13.74	9.29	0.00	0	0	9.2839	Periodic	(1)
J16081050-2351024	204054556	02	16:08:10.509	-23:51:02.44	F3V	1	9.17	7.83	1.00	1	0	109.3195	Periodic/Long-term	(1)
J16081081-1904479	205164832	02	16:08:10.824	-19:04:48.00	K3IVe	0	12.29	8.47	1.00	1	0	3.0627	Periodic	(3)
J16081474-1908327	205152548	02	16:08:14.700	-19:08:31.99	K2	0	11.73	8.43	1.00	1	0	10.6598	Periodic	(1)
J16082234-1930052	205080360	02	16:08:22.344	-19:30:05.22	M1	0	13.86	9.06	0.00	0	1	2.3829	Periodic	(1)
J16082324-1930009	205080616	02	16:08:23.244	-19:30:00.93	K9	1	14.03	9.47	0.00	0	1	2.3829	Periodic	(1)
J16082511-2012245	204932100	02	16:08:25.108	-20:12:24.58	M1	0	14.19	9.87	0.00	0	0			(1)
J16083436-1911563	205141287	02	16:08:34.298	-19:11:54.99	K5	0	12.17	7.79	1.00	1	0	7.7576	Periodic	(3)
J16083514-2045296	204810792	02	16:08:35.140	-20:45:29.62	F3V	0	8.36	6.68	0.00	0	0			(1)
J16084340-2602168	203468205	02	16:08:43.298	-26:02:16.00	G8	0	10.28	7.91	1.00	1	0	2.1912	Periodic	(1)

Table 1: continued

J16084366-2522367	203660895	02	16:08:43.668	-25:22:36.62	F4V	0	8.81	7.25	0.00	0	0	3.9124	Periodic	(1)
J16090075-1908526	205151387	02	16:09:00.729	-19:08:52.58	K9	1	13.79	9.15	0.00	0	0	9.7017	Periodic	(1)
J16090844-2009277	204942552	02	16:09:08.445	-20:09:27.79	M4	0	14.10	9.52	0.00	0	0			(1)
J16091373-2001045	204972242	02	16:09:13.696	-20:01:04.00	G4	0	11.42	9.54	0.00	0	0			(4)
J16092918-1852536	205203376	02	16:09:29.184	-18:52:53.76	K4IVe	0	12.73	8.38	0.00	0	0			(3)
J16093035-2443379	203842174	02	16:09:30.357	-24:43:37.92	M3.5	0	14.02	9.50	0.00	0	0			(1)
J16093164-2229224	204398857	02	16:09:31.660	-22:29:22.41	M2.0	1	13.23	9.15	0.00	0	0			(2)
J16093969-2200466	204518032	02	16:09:39.700	-22:00:46.62	M0.5	0	13.47	9.30	0.00	0	0	6.5025	Periodic	(2)
J16094644-1937361	205054287	02	16:09:46.440	-19:37:36.08	M1	0	14.21	9.63	0.00	0	0			(1)
J16095441-1906551	205157836	02	16:09:54.420	-19:06:55.00	M1	1	14.39	9.60	0.00	0	0	16.2387	Periodic	(1)
J16100501-2132318	204630363	02	16:10:05.016	-21:32:31.88	M0.0	1	13.04	8.95	0.00	0	0	6.6224	Periodic	(2)
J16101729-1910263	205146246	02	16:10:17.304	-19:10:26.40	K5IVe	0	12.72	8.53	0.00	0	0			(3)
J16102653-2756293	202904813	02	16:10:26.544	-27:56:29.40	M3Ve	0	13.93	9.57	0.00	0	0			(3)
J16102857-1904469	205164892	02	16:10:28.576	-19:04:46.99	M3	1	13.69	8.71	0.00	0	0	6.6657	Periodic	(1)
J16102888-2213477	204464828	02	16:10:28.879	-22:13:47.78	G7IVe	0	9.71	7.23	1.00	1	0	2.2922	Periodic/Long-term	(1)
J16103196-1913062	205137430	02	16:10:31.960	-19:13:05.98	K7	0	13.51	8.99	0.00	0	0	12.3305	Periodic	(1)
J16110479-2333166	204127977	02	16:11:04.797	-23:33:16.59	M0.0	0	13.38	9.66	0.00	0	0	4.8760	Periodic	(2)
J16110890-1904468	205164889	02	16:11:08.908	-19:04:46.84	K2	0	12.05	7.69	1.00	1	0	3.7946	Periodic	(1)
J16112601-2631558	203318214	02	16:11:26.028	-26:31:55.88	M2.0	1	14.43	9.57	0.00	0	0			(2)
J16114387-2526350	203641931	02	16:11:43.872	-25:26:35.16	K3IV(e)	0	11.77	8.74	0.00	0	0	8.7973	Periodic	(3)
J16115266-2232421	204384743	02	16:11:52.658	-22:32:42.10	A3V	0	8.24	7.27	0.00	0	0			(1)
J16115633-2304051	204251947	02	16:11:56.294	-23:04:04.00	M1	0	12.71	8.81	1.00	1	0	5.4915	Periodic	(1)
J16115927-1906532	205157937	02	16:11:59.277	-19:06:53.28	K0	0	11.59	8.09	1.00	1	0	3.6157	Periodic	(1)
J16120505-2043404	204817605	02	16:12:05.049	-20:43:40.51	M1.0	1	13.74	9.06	0.00	0	0	9.3735	Periodic	(2)
J16123531-2034339	204851310	02	16:12:35.323	-20:34:33.99	M0.5	0	13.73	9.30	0.00	0	0			(2)
J16123604-2723031	203063710	02	16:12:36.052	-27:23:03.19	K4.0	0	11.26	7.23	0.00	0	0			(2)
J16124051-1859282	205182220	02	16:12:40.512	-18:59:28.28	K6	0	10.97	7.49	1.00	1	0	1.5224	Periodic	(1)
J16124123-1949380	205012599	02	16:12:41.236	-19:49:38.02	M1	0	13.39	8.90	0.00	0	0	3.6293	Periodic	(1)
J16124682-2213317	204465961	02	16:12:46.824	-22:13:31.80	K3IV(e)	0	11.20	8.03	0.00	0	1	10.6760	Periodic	(3)
J16125533-2319456	204185181	02	16:12:55.334	-23:19:45.69	G2V	1	9.36	7.29	0.00	0	0	4.2582	Periodic	(1)
J16130271-2257446	204279085	02	16:13:02.700	-22:57:42.98	K4.5	0	11.72	8.46	0.00	0	0	2.1012	Periodic	(1)
J16131158-2229066	204399980	02	16:13:11.584	-22:29:06.68	A8III/IV	1	8.87	6.69	1.00	1	0		Dipper	(1)
J16131858-2212489	204468888	02	16:13:18.499	-22:12:48.02	K0	0	10.40	7.43	1.00	1	0	5.8812	Periodic	(1)
J16133644-2326270	204156820	02	16:13:36.441	-23:26:26.98	M2.5	0	14.07	9.31	0.00	0	0			(2)
J16134366-2214594	204459941	02	16:13:43.656	-22:14:59.64	K7IVe	1	13.22	9.11	0.00	0	0	4.6731	Periodic	(3)
J16134781-2747340	202947197	02	16:13:47.820	-27:47:34.00	F4.5	1	9.30	8.01	0.00	0	0			(2)
J16140733-2217321	204449165	02	16:14:07.348	-22:17:32.20	M1.0	0	13.33	9.10	0.00	0	0	0.6178	Periodic	(2)
J16141107-2305362	204245509	02	16:14:11.001	-23:05:35.01	K2	1	10.71	7.46	1.00	1	0	35.8945	Periodic/Dipper	(1)
J16145918-2750230	202933888	02	16:14:59.203	-27:50:22.02	G8	1	10.98	8.69	1.00	1	0	4.3735	Periodic	(1)
J16150927-2345348	204076987	02	16:15:09.280	-23:45:35.02	F3V	1	9.49	8.03	0.00	0	0			(1)
J16151948-2540119	203576256	02	16:15:19.488	-25:40:12.00	M1.5	0	14.30	9.12	0.00	0	0	0.6985	Periodic	(2)
J16153215-2530310	203623026	02	16:15:31.996	-25:30:29.98	G2	0	10.73	8.24	0.00	0	0	2.5721	Periodic	(4)
J16153311-2707587	203136724	02	16:15:33.110	-27:07:58.80	M0.5	0	14.02	9.76	0.00	0	0	3.2574	Periodic	(2)

Table 1: continued

J16153587-2529008	203630298	02	16:15:35.856	-25:29:00.99	K5	0	12.89	8.74	0.00	0	0	1.8903	Periodic	(1)
J16162191-2809504	202842502	02	16:16:21.919	-28:09:50.47	A1	0	9.13	7.93	0.00	0	0			(1)

[†]References: (1) = [Luhman & Mamajek \(2012\)](#), (2) = [Rizzuto et al. \(2015\)](#), (3) = [Pecaut & Mamajek \(2016\)](#) (4) = [Preibisch et al. \(1998\)](#)

[‡]Sources with periods that would have been rejected as potential aliases (see Section 2.3.2) but were kept due to clear periodicity in the KELT data or confirmation of the period from *K2/C2*.

This paper has been typeset from a $\text{T}_\text{E}\text{X}/\text{L}^\text{A}\text{T}_\text{E}\text{X}$ file prepared by the author.